Cyclobutane-linked Nanothreads through Thermal and Photochemically Mediated Polymerization of Cyclohexadiene

Morgan Murphy,[†] Bohan Xu,[⊥] Katie E. Rank, [‡] Sikai Wu,[†] Steven Huss,[†] John V. Badding,[†,⊥,§,‖] Steven A. Lopez,[‡] Vincent H. Crespi,[†,⊥, §,‖] and Elizabeth Elacqua*[,†]

[†] Department of Chemistry, The Pennsylvania State University, University Park, PA, 16802.

[⊥] Department of Physics, The Pennsylvania State University, University Park, PA, 16802.

[‡] Department of Chemistry and Chemical Biology, Northeastern University, Boston, MA, 02115.

[§] Materials Research Institute, The Pennsylvania State University, University Park, PA, 16802.

[‖] Department of Materials Science and Engineering, The Pennsylvania State University, University Park, PA, 16802.

ABSTRACT: Carbon nanothreads are a rapidly growing class of 1D nanomaterials with sp^3-hybridized diamond-like backbones. Most nanothreads are synthesized through the pressure-induced polymerization of aromatics, resulting in diverse structures and functionalities. Aside from precursor selection, there are currently limited means to control nanothread reaction pathway or polymerization outcome. Analogous to selection rules that govern outcomes in small molecule chemistry, we investigated both thermally and photochemically mediated polymerizations of skipped and conjugated dienes (1,3- and 1,4-cyclohexadiene) under high pressure and explored the resultant product selectivity. For 1,3-cyclohexadiene, both approaches yield largely amorphous products owing to competing reaction pathways. Thermally mediated polymerization of 1,4-cyclohexadiene yields a crystalline product; however, the identification of the backbone composition is consistent with multiple different reaction pathways being accessible. While support for cyclobutane structures is present, comparison to the simulated structures suggests multiple products are obtained from the thermal polymerization of 1,4-cyclohexadiene. In contrast, the recovered product obtained from photochemically mediated polymerization of the skipped diene has different *d*-spacings and is consistent with simulations that support a single reaction pathway toward cyclobutane-linked nanothreads. These results suggest that photochemical activation can enable product selectivity in nanothread synthesis.

INTRODUCTION

Pressure-induced polymerizations of unsaturated cyclic precursors has often yielded amorphous hydrocarbon networks.[1-5] Recently, the high-pressure polymerization of aromatics realized a new class of materials – called nanothreads – when the slow solid-state compression of benzene afforded a distinct crystalline product.[6, 7] Nanothreads are synthesized through kinetically controlled polymerization, wherein reactions apparently occur along stacks in a molecular crystal.[6-29] NMR spectra obtained for benzene- and furan-derived nanothreads supported polymerization through repeated [4+2]-cycloadditions.[13, 15] In contrast, cubane-derived nanothreads were the result of radical polymerization.[10] Whereas these solid-state reactions are dictated by the arrangement of precursor molecules,[17-23] methods to select specific reaction pathways and access new architectures remain largely unstudied.

In solution-based and solid-state organic synthesis, heat and light are often used to achieve different products. For pericyclic reactions within thermal and photochemical systems, orbital symmetry and the Woodward-Hoffmann selection rules help predict stereospecific reaction outcomes.[30] For example, the electrocyclic ring opening of substituted cyclobutenes results in different stereoisomers under photochemical and thermal conditions. Translating this concept to macromolecular systems, in particular carbon-based nanothreads, could enable different mechanisms and stereochemical outcomes to be achieved. Moreover, the use of photochemistry to direct nanothread formation may realize alternate architectures and/or facilitate reactivity in previously inert nanothread systems.

Recently, photochemical irradiation was reported to reduce the pressures required for polymerization into nanothreads.[9, 31] For example, monomeric pyridine formed well-ordered sp^3-rich products using laser or broadband irradiation. The use of photochemistry in the polymerization of furan also afforded nanothreads at reduced pressures; quantum mechanical calculations revealed that the reaction favored a photochemically accessible [4+4]-cycloaddition as the initiation step[9] in contrast to thermally governed polymerizations, thus enabling propagation through more energetically favorable [4+2]-cycloadditions. While the introduction of light to access a structurally diverse array of 1D polymers is well-studied,[32-39] leveraging photochemistry to selectively dictate polymer structure (compared to thermal means) in strict analogy to molecular systems has yet to be documented.

Here we investigate isomers of cyclohexadiene as monomers for pressure-induced polymerization. We hypothesize that the nature of the diene – conjugated or skipped – would dictate which mechanisms and products might be accessible from the polymerization, while expecting different pathways compared to benzene.[40] Moreover, the comparative reactivities of 1,3- and

1,4-cyclohexadiene may help elucidate polymerization outcomes. While the conjugated diene is considered more stable owing to resonance, the cyclization of hexadiene is destabilizing, leading to higher energy in the corresponding π orbitals. Consequently, the thermal dimerization of 1,3-cyclohexadiene yields a mixture of products from competing [4+2]-cycloaddition, [2+2]-cycloaddition, and [6+4]-ene reactions.[41-43] In contrast, cyclization of the skipped diene is overall stabilizing owing to hyperconjugation. Thus, we hypothesize that pressure-induced polymerization of 1,3-cyclohexadiene might initiate at lower pressures but is unlikely to favor one reaction pathway. In contrast, the heightened stability of 1,4-cyclohexadiene suggests it might require higher pressures to induce reactivity from fewer viable reaction pathways.[44]

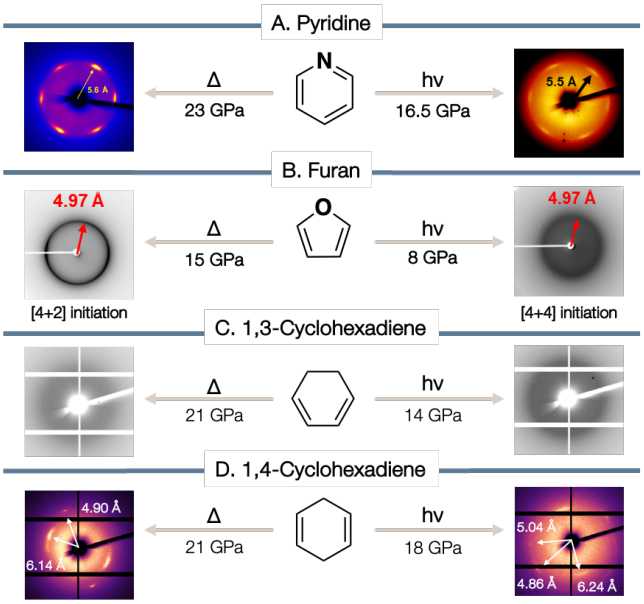

Figure 1. Summary of reported ambient temperature and photochemically mediated polymerizations of pyridine and furan, wherein substantial reductions in pressure were observed, and cyclohexadiene isomers, wherein distinct structural outcomes are achieved using the two methods.

In studying 1,3- and 1,4-cyclohexadiene we also became interested in using our polymerization method based on UV-irradiation[9] to investigate the possibility of new mechanisms and/or specific product formation. Previous photochemical dimerizations of 1,3-cyclohexadiene have observed a mixture of products, with the results suggesting that the [2+2]-cycloaddition pathway outcompetes [4+2]-Diels-Alder dimerization. Photochemical dimerizations of substituted 1,4-cyclohexadienes, although lesser studied, result predominantly in cyclobutane linkages.[45] Photochemical irradiation may decrease the reaction pressures required for polymerization at ambient temperature. Photochemically mediated polymerization may also yield a more ordered product from 1,3-cyclohexadiene, owing to reduced pathways available through dimerization. Since fewer pericyclic reactions are observed using 1,4-cyclohexadiene, we hypothesize that thermally and photochemically mediated polymerizations of it may afford different products. Our hypotheses, while in analogy to conventional organic chemistry, are in sharp contrast to non-pressure-induced polymerizations wherein heat and light are less known to affect reaction mechanism.

Monomeric 1,3-cyclohexadiene was expected to react given the conjugated diene's propensity for both [4+2]-cycloadditions and photopolymerization in conventional systems. Despite the built-in reactive diene, we find that the application of pressure is unable to achieve an ordered product. The addition of UV irradiation affords a product with weak diffraction. In contrast, polymerization of 1,4-cyclohexadiene at room temperature affords an ordered polycrystalline solid, evidenced by X-ray diffraction, while the photochemically mediated polymerization of 1,4-diene achieves a distinct product at reduced pressures.

RESULTS AND DISCUSSION

Thermally Mediated Pressure-induced Reactivity of 1,3-Cyclohexadiene

Polymers of 1,3-cyclohexadiene (1,3-diene) have been obtained through many mechanisms including cationic,[46] anionic,[47, 48] radical,[49] and Ziegler-Natta[50] polymerization. We hypothesized that the 1,3-diene could polymerize through a series of [4+2]-cycloaddition reactions analogous to degree-4 nanothreads[7, 13, 18, 40, 51] derived from aromatic precursors such as benzene and furan.[13, 15] Whereas non-aromatic π-bond-containing molecules have not been explored for nanothread formation, we posited that the conjugated cyclic diene may enable facile [4+2]-cycloadditions to be achieved.

The thermal pressure-induced reactivity (20–22˚C) of 1,3-diene was studied through in situ Raman and infrared (IR) spectroscopy (Figures 2 and S1). Liquid 1,3-diene was loaded into a diamond anvil cell (DAC), where it solidified into a glassy phase at approximately 1.5 GPa, as confirmed by a lack of lattice modes observed in the Raman spectrum. A glassy sample of 1,3-diene was compressed to a maximum pressure of 20–21 GPa, held at this pressure overnight, then decompressed over 7 hours whereupon an opaque solid was recovered (Figure S8).

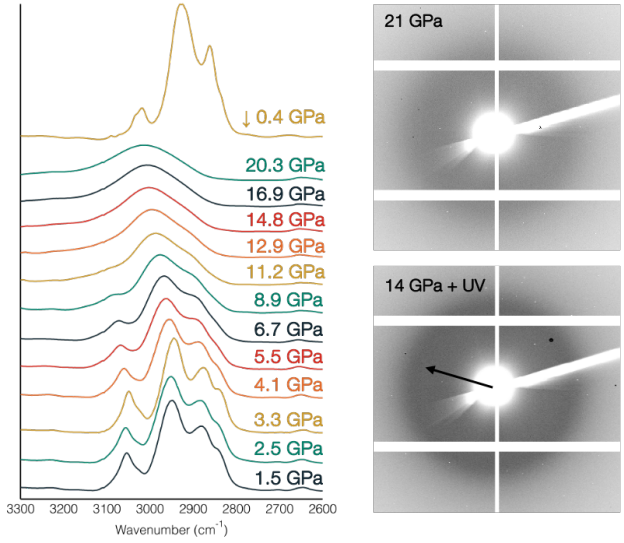

Figure 2. Left: In situ IR spectral overlay highlighting C–H stretching modes taken throughout the compression to 20 GPa of 1,3-diene. Right: Synchrotron powder X-ray diffraction of the product recovered after compression to 21 GPa (top), or 14 GPa with UV light exposure (bottom).

In situ Raman spectroscopy revealed that a reaction had taken place under pressure, evidenced by a large increase in the photoluminescent (PL) background beginning at 11 GPa (Figure S1).[7, 16, 23] The broad vibrational modes of 1,3-diene at low

pressure matched the reported low temperature spectra.[52 53] Another experiment using in situ IR spectroscopy showed no changes that suggested a phase transition to the molecular system, as consistent relative intensities between modes are seen throughout the compression (Figure S5). Furthermore, the precursor C(sp^3) modes broadened and increased in intensity. The sizable shifts and changes in the vibrational modes indicated a different chemical environment for the product and supported a reaction under pressure.

Upon decompression and recovery of the polymerized material, shifts in the sp^3 and sp^2 C—H stretching modes were observed: IR modes at 3054 cm^{-1}, 2948 cm^{-1}, and 2881 cm^{-1} in the precursor shifted to 3018 cm^{-1}, 2927 cm^{-1}, and 2861 cm^{-1} respectively in the recovered product. The integrated areas of the sp^2 and sp^3 C—H regions of the product spectrum were used to estimate the ratio of C(sp^3):C(sp^2).[2] From this analysis, the solid recovered from the in situ IR compression to 20 GPa had an estimated 88% sp^3 carbon content. Synchrotron X-ray diffraction of recovered samples showed no distinct features, indicative of an amorphous product (Figure 2). We attributed this to competing pericyclic reactions that enabled high C(sp^3) content to be achieved despite an ill-defined structure and/or packing.

Photochemically Mediated Pressure-induced Reactivity of 1,3-Cyclohexadiene

Given the possibility of selecting accessible reactions, we explored the pressure-induced reactivity of 1,3-diene with UV irradiation in a DAC. Samples of 1,3-diene were exposed to broadband UV light while being compressed and monitored by in situ Raman spectroscopy. Raman spectra revealed a notable decrease in the reaction onset pressure (from 11 GPa to 5 GPa), evidenced by the PL background beginning at lower pressure (Figure S1). However, the introduction of UV light did not impact the peak position or reduce broadness, affording a spectrum that appeared analogous to thermal polymerization.

The IR spectra of products obtained from thermally and photochemically mediated compressions of the 1,3-diene featured subtle differences in the fingerprint region (Figure S3). In the photochemical sample, a broad peak appeared at 1357 cm^{-1} akin to the thermal sample (Figure S3), which was attributed to the formation of new C—H stretching modes. However, the photochemically generated product featured several distinct modes at 1308 cm^{-1}, 887 cm^{-1}, and 878 cm^{-1} that we tentatively assigned to C–H stretching and alkyl ring vibrations. Raman and IR spectroscopy indicate that irradiation with UV light led to the formation of a sp^3 hybridized product.[54] In contrast to thermal compressions, powder X-ray diffraction of the product obtained using photochemically mediated polymerization shows a diffuse ring at 5.2 Å (Figure 2), suggesting the photochemically mediated reaction selected for the more conventional [4+2]- and [2+2]-cycloadditions as seen in molecular systems. Thus, a more ordered solid was obtained wherein the *d*-spacing was consistent with a polycrystalline nanothread-like product. From the data obtained we cannot rule out ring-opening reactions or integration of ring-opened products within the final polymer structure.

Overall, UV irradiation during compression of 1,3-diene decreased the reaction pressure while enabling the formation of a semi-ordered product with high C(sp^3) content. Our observations suggest that photochemistry limits the accessible pathways, leading to more selective polymerization reactions. These results align well with the molecular dimerization of 1,3-diene.

Thermally Mediated Pressure-induced Reactivity of 1,4-Cyclohexadiene

Unlike 1,3-cyclohexadiene, 1,4-cyclohexadiene (1,4-diene) does not contain a conjugated diene, but rather a skipped diene. Thus 1,4-diene does not contain the generally accepted diene required for Diels-Alder cycloadditions that often characterize nanothread formation.[13, 15] Without a conjugated system, the 1,4-diene may realize new architectures from polymerization through reactions such as pericyclic and radical [2+2]-cycloadditions. We calculated the reaction free energies associated with oligomerization through theoretical reactions (see SI) resulting in partially and fully saturated structures attainable through Zigzag (ZZ), Armchair (AC), and Cyclobutane (CB) pathways (Figure 3). Our calculations suggest that propagation through [2+2]-cycloadditions toward cyclobutane-linked structures is thermodynamically favorable when the reacting molecules of 1,4-diene are staggered. Further, the radical mechanistic pathways that AC or ZZ architectures would encounter are disfavored upon initiation, although lower relative energies occur upon further oligomerization. The results of these calculations are shown in Figures S27 and S28.

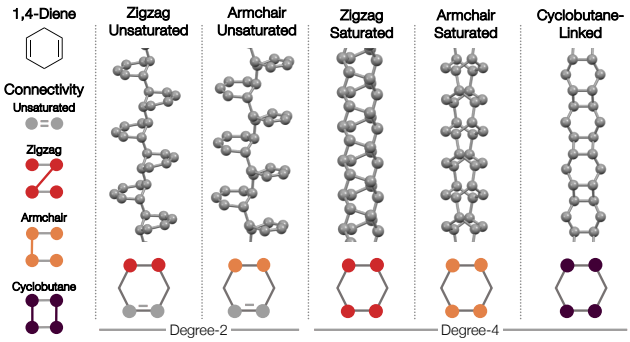

Figure 3. Possible structural outcomes from a one-dimensional polymerization of 1,4-cyclohexadiene with different connectivity patterns.

The pressure-induced polymerization of 1,4-diene was first investigated at 20–22˚C in a DAC without UV irradiation. Loaded 1,4-diene solidified at approximately 1.5 GPa into a polycrystal. Attempts to grow single crystals in the DAC through annealing at low pressure or cooling still resulted in polycrystalline samples. Samples of polycrystalline 1,4-diene were compressed to a maximum pressure of 21 GPa and held at this pressure overnight. Upon decompression a white solid was recovered (Figure S8).

In situ IR spectroscopy showed broadening and shifting of C–H stretching modes at increased pressures (Figure 4). In addition, all vibrational modes broadened with increased pressure, while the sp^2 stretching modes decreased in intensity between 14 and 15 GPa, indicating the start of a reaction. This observation suggests that the skipped diene required higher pressures compared to the conjugated diene, in line with our expectations. After decompression, stretching in the C–H sp^2 region softened to lower wavenumbers (from 3054 to 3017 cm^{-1}) while the sp^3

stretching modes from 2948 to 2881 cm^{-1} merged into a broad peak centered at 2917 cm^{-1}. Additional vibrational modes were observed at 1035 and 1475 cm^{-1} which likely correspond to ring breathing modes and new sp^2-sp^3 bending modes, consistent with a reaction under pressure (Figure S4). The prominent HC=CH bending modes of the precursor at 617 and 1160 cm^{-1} were absent in the recovered spectrum at 0 GPa, which confirmed consumption of the skipped diene reactant. The IR spectrum of the product suggested that ~80% of the carbon atoms are sp^3 hybridized.[2]

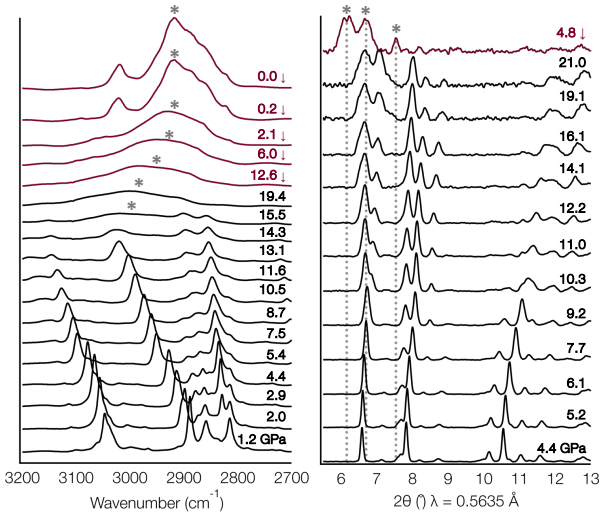

Figure 4. In situ monitoring of separate compressions of 1,4-diene to 21 GPa through (left) IR spectroscopy and (right) synchrotron powder X-ray diffraction. Red spectra were collected on decompression (also denoted with downward arrows) and asterisks denote new peaks.

In a separate experiment, in situ Raman spectra were recorded to monitor the reaction progress of a polycrystalline sample of 1,4-diene held at the maximum pressure of 21 GPa for 24 hours. An increased PL background was observed between 11 and 15 GPa (Figure S2), which is often indicative of a chemical change. Above 15 GPa no vibrational modes could be discerned over the PL background. A phase transition was seen with in situ Raman spectroscopy. This was supported by new vibrational modes appearing as low as 1.5 GPa and continuing to 6 GPa, at which point the sample no longer matched the reported ambient pressure Raman spectra for 1,4-diene.[55] Synchrotron XRD of the recovered sample showed two interplanar spacings with $d_{24\text{-hour}}$ = 6.04 and 5.83 Å (Figure 5, right panel).

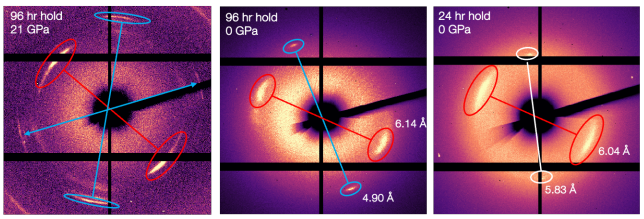

Figure 5. Recovered gasket diffraction from experiments that polymerized at the max pressure for 96 hours and 24 hours.

To further investigate the polymerization of the 1,4-diene, a powder sample was monitored through in situ synchrotron powder X-ray diffraction (Figure 4). The 1,4-diene was compressed at a controlled rate of 5 GPa per hour to a final pressure of 21 GPa, followed immediately by decompression to ambient pressure at the same rate. New diffraction peaks emerged on decompression at approximately 10 GPa. Peaks corresponding to three distinct interplanar spacings (that are inconsistent with solidified 1,4-diene) increased in intensity as the pressure dropped. The product of the in situ powder experiment was crystalline on decompression until 4.8 GPa, where the sample lost order (Figure S7). The loss of order might be owing to incomplete polymerization and/or the formation of shorter less stable structures. We, thus, sought to investigate an additional compression using in situ XRD, wherein the sample was held at the maximum pressure for an extended time prior to decompression.

Polycrystalline 1,4-diene was compressed to 21 GPa and held at that pressure for 96 hours. The decompression was monitored through XRD, with scans being recorded every 1–2 GPa (Figure 7). Here, we observed the expansion of the interplanar spacings, along with significant relative expansion observed over the last 2 GPa. We recovered a crystalline product with two interplanar spacings, $d_{96\text{-hour}}$ = 6.14 Å and 4.90 Å (Figure 5). The recovery of one large and one small *d*-spacing suggests a product with anisotropic packing (Figure 6).

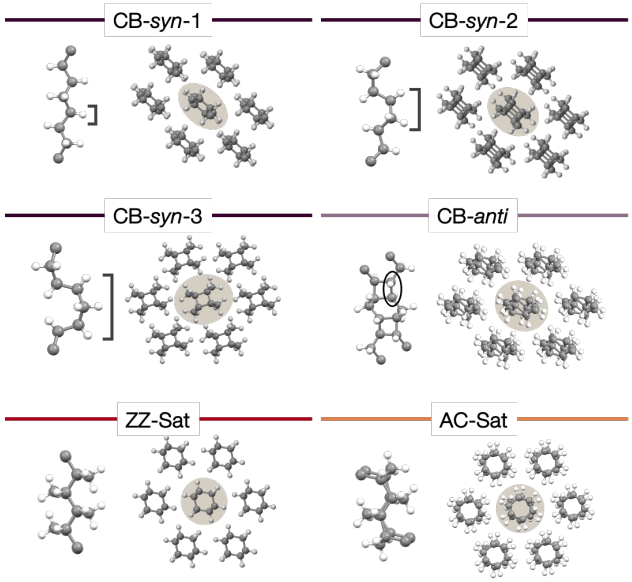

Figure 6. Simulated structures and anisotropic packings relaxed at 0 K and 0 GPa. The number of consecutive hydrogens (shown with brackets) along the backbone is used to differentiate CB-*syn* packings. The *anti*-pair of hydrogens is circled in the CB-*anti* structure.

Simulated Diffraction and Nanothread Packings for Thermal Compressions of 1,4-Cyclohexadiene

To further investigate the resulting sp^3-hybridized and crystalline product, decompression data from the in situ XRD experiment (the 96-hour sample) was compared to the simulated diffraction of 1,4-diene-derived materials geometrically optimized through ab-initio computation with PBE functional,[56] DFT-D3/BJ van der Waals correction,[57, 58] and plane wave basis set, implemented in the VASP package.[59-63] All possible nanothread structures with an axial unit cell containing one or two precursor molecules without significant strain, hydrogen migration, or intramolecular bond breaking were considered. The simulated structures included both degree-2 (unsat) and degree-4 (sat) nanothreads of Zigzag (ZZ-unsat and ZZ-sat) and

Armchair (AC-unsat and AC-sat) connectivity, along with cyclobutane (CB)-links, and crosslinked materials. Sixteen different packing geometries were randomly generated for each thread species. After geometry relaxation, those initial packing geometries converged to one or two low-enthalpy packings for each thread species, which are then compared to the experimental *d*-spacings. (See SI for simulated structures and packings not included in Figure 7).

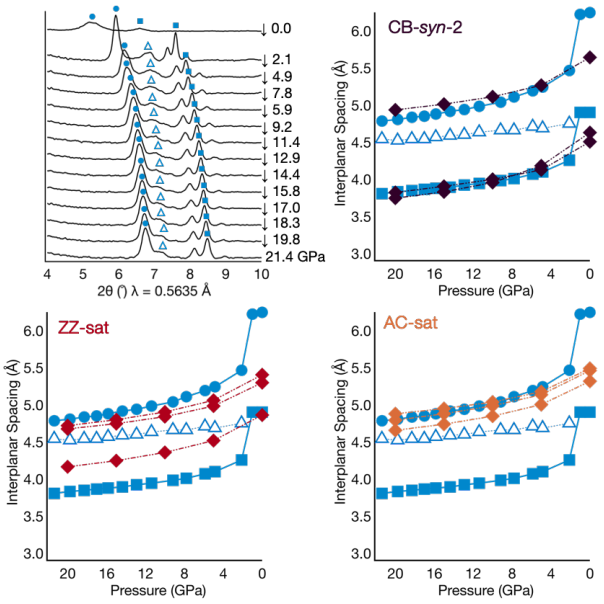

Figure 7. Experimental (96-hour sample) and simulated X-ray diffraction data for 1,4-diene: (top left) overlay tracing decompression of polymerized 1,4-diene with blue circles, blue squares, and blue triangles highlighting relevant peaks and comparison of experimental *d*-spacing to simulated diffraction data for (top left) CB-*syn*-2 packing, (bottom left) ZZ-sat packing, and (bottom right) AC-sat packing.

Some categories of structural candidates are easily eliminated due to significant disagreement between simulated *d*-spacings and the experimental data. For example, the simulated diffraction for sheet-like products (Figure S25 and S26) deviated significantly from the experimental decompression data, so structures of this dimensionality could be excluded. To examine the nanothread candidates, we assume the observed reaction product Friedel pairs are associated with the two-dimensional lattice of thread packing; such peaks are typically much more easily observed than those from axial periodicity, presumably due to longer-ranged structural order in the packing direction. The non-rigid degree-2 (unsat) structures each have two distinct conformations (eclipsed and staggered). The unsat staggered conformations yield one d-spacing exceeding 7.0 Å, which is excluded by the experimental data. The unsat eclipsed conformations are more than 0.7 eV higher in enthalpy per precursor than the staggered conformations (a difference not overcome by PΔV enthalpy differences at the reaction pressure). Furthermore, these two structures are conformational isomers and thus eclipsed may convert to staggered at ambient pressure, so the unsat eclipsed conformation is also ruled out.

The remaining possible thread candidates include the CB-*syn*, CB-*anti*, ZZ-sat, and AC-sat structures. CB-*syn* threads would be formed from propagating [π2s + π2s]-cycloadditions which are traditionally understood as symmetry-forbidden.[64] In contrast, CB-*anti* threads would be formed from [π2s + π2a]-cycloadditions, which are symmetry-allowed under thermal conditions. However, they are 0.25 to 0.5 eV higher in enthalpy per precursor and more than 0.4 eV higher in gas phase dimerization reaction barrier than CB-*syn* threads. The dimerization barrier is computed by slow-growth method [ref] implemented through VASP.[65-67] The alignment needed for [π2s + π2a] reaction is also hard to achieve due to steric constraints at high pressure. Therefore, the CB-*anti* outcome is less likely than CB-*syn* despite CB-*anti* having a symmetry-accessible [π2s + π2a] reaction trajectory. For the CB-*syn* structures simulated, the number following the conformation indicates the number of consecutive hydrogen pairs along one side of the nanothread backbone. For instance, CB-*syn*-3 has three consecutive hydrogen pairs along one side of the thread, accumulating curvature and thus manifesting a more circular nanothread cross-section in projection along the axis (Figure 6). The lack of curvature accumulation in the CB-*syn-1* thread produces a more elliptical cross-section.

We compare the remaining structures and their simulated diffraction data with the in situ XRD data for decompression from 21 GPa (Figure 7). Unmarked peaks at approximately 8 and 9 2θ were attributed to the precursor and not analyzed further. The *d*-spacings marked by solid blue circles and solid blue squares are taken to arise from the two-dimensional lattice of thread packing. The combination of a long (blue circle) and short (blue square) *d*-spacing indicated a degree of ellipticity only achievable by CB-threads with one or two consecutive hydrogens alternating sides along the thread (Figure 5). A weak set of Friedel pairs with the same *d*-spacing as the blue squares was observed at 21 GPa but not at ambient pressure. Having two sets of similarly spaced Friedel pairs is consistent with the CB-threads having two short *d*-spacings in simulations (Figure 7 and S10). A weaker and broader peak marked with a hollow blue triangle, which is close to a peak of the precursor molecular crystal, disappeared at ambient pressure (Figure 7). Its variation in *d*-spacing under decompression also differs from those of *d*-spacings associated with thread packing. Therefore, this hollow triangle peak was not included in the analysis of thread packings. Considering the solid circle and square peaks, the *d*-spacings from the 96-hour sample matched well, at all pressures, with the simulated CB-threads whose ellipticity corresponded to having one or two consecutive hydrogens alternating on the two sides of a thread (Figures S13 to S26). The abrupt expansion step as pressure is released is characteristic of other nanothread samples[16] and is attributed to a release of pressure-induced straightening of the threads around on-thread structural defects (the disorder associated with this "destraightening" may account for the unobservability of the second short *d*-spacing upon recovery).

The XRD obtained on the 24-hour sample (Figure 5), lacked short *d*-spacings, suggesting a reaction product different from the 96-hour sample. Such *d*-spacings are consistent with threads with less elliptical cross-section, such as AC-sat, ZZ-sat, and CB-threads with at least three consecutive hydrogen pairs along one side (e.g., CB-*syn-3*). Although the AC-sat thread aligns best with the two observed d-spacings, the absence of an expected third set of quasi-hexagonal Friedel pairs and the lack of in-situ XRD data for this 24-hour sample prevent a more confident identification of its reaction product.

Overall, the thermally mediated polymerization of 1,4-cyclohexadiene likely produced either CB-nanothreads with incomplete XRD peaks (as in the 96-hour sample) or other distinct reaction products (as in the 24-hour sample). In contrast, we will show that the high-pressure polymerization under photochemically mediated conditions produced a more ordered thread that retains all Friedel pairs to ambient pressure and showed a highly elliptical cross-section associated with CB-threads.

Photochemically Mediated Pressure-induced Reactivity of 1,4-Cyclohexadiene

To explore alternate reaction pathways, and/or reduce reaction pressures photochemically, polycrystalline samples of 1,4-diene were compressed while being irradiated with UV light in a DAC. Several conditions were explored, with variations including changing the maximum pressure (GPa) and exposure time (hours) for the samples. Methods introducing UV irradiation for a specific amount of time at various pressure points or continuous UV light exposure throughout slow compression were investigated. Experiments which used three hours of broadband UV irradiation at various pressure points throughout the experiment afforded the most crystalline solids. Recovered samples from these experiments to 12, 14, 15, and 18 GPa produced semi-crystalline solids; however, the 12 GPa samples did not diffract (Figure S7). Those compressed to 10 GPa or below crystallized under pressure but reverted to a liquid after UV light exposure and decompression.

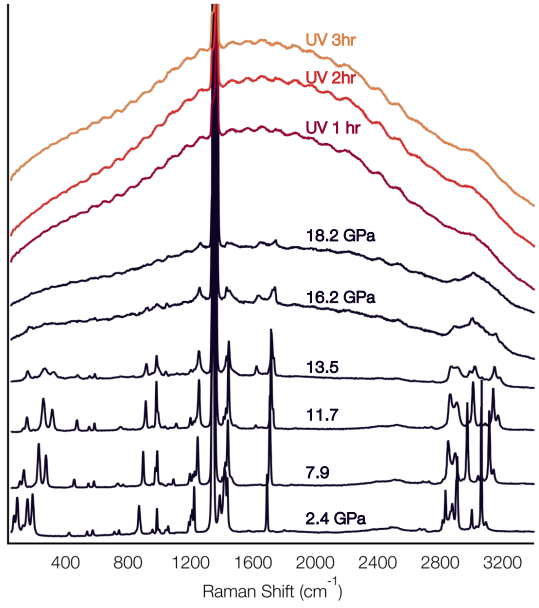

Figure 8. In situ Raman spectral overlay of the photochemically mediated compression of 1,4-diene to 18 GPa along with subsequent Raman scans after each 1-hour irradiation period.

In our optimal experiments, samples of liquid 1,4-diene were compressed to 18 GPa over three hours and allowed to equilibrate overnight. In situ Raman spectroscopy was used to monitor reaction progress. At 18 GPa, the sample was exposed to UV light in one-hour increments after which Raman scans were taken immediately; samples were irradiated for a total of three hours at that pressure. Raman spectra showed broadening of the 1,4-diene vibrational modes under pressure, with a slight increase in the PL background being observed at the maximum pressure of 18 GPa (Figure 8). Scans after each hour of UV irradiation showed a large increase in the PL background, likely resulting from chemical transformation.

IR spectra of the recovered solid featured an intense C–H stretching peak below 3000 cm^{-1} (Figure S4), along with new vibrational modes at 1035 and 1475 cm^{-1} which likely correspond to a ring breathing mode and new sp^2-sp^3 bending modes. Collectively, these suggest that the sample underwent a successful reaction.

Synchrotron X-ray diffraction of recovered gasket samples shows a pseudo-hexagonal diffraction pattern with *d*-spacings belonging to the nanothread lattice at 6.24, 5.04, and 4.86 Å (Figure 9). Recent accounts of photochemically mediated nanothread synthesis saw a reduction in reaction pressure but yielded the same or very similar *d*-spacings as/to those of non-irradiated samples.[9,31] Here, the introduction of photochemistry resulted in a product with *d*-spacings which are distinct from those obtained through thermal compressions.

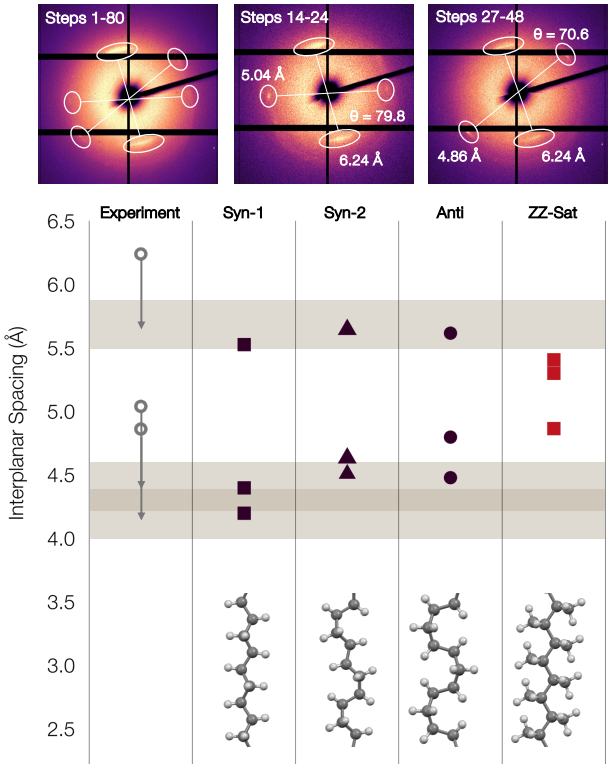

Figure 9. Synchrotron X-ray diffraction of 1,4-diene compressed to 18 GPa with 3 hours of UV light (accumulation of steps 80 scans highlighting Friedel pairs (scans 14-24 and 27-48)) and comparison of experimental and simulated *d*-spacings. The shaded bands show a 0.5–0.8 Å adjustment accounting for destraightening and thermal expansion (see main text).

These obtained *d*-spacings can be compared to the simulated candidate structures and packings (Figure 9). The observation of one large and two smaller *d*-spacings in the experimental data suggested that nanothreads with elliptical cross-sections and CB linkages are the reaction product. The diffraction image of the reaction product shows the three Friedel pairs expected for the first-order diffraction spots of a quasi-hexagonal thread

packing, in contrast to the thermal reaction product which only shows two pairs. Thus, an increase in structural order is obtained under photochemical conditions. The photochemical reaction product also lacks the 5.83 Å peak that was observed in the thermal reaction product (Figure 5, 24-hour sample). The combined data suggests that the photochemical conditions select a singular mechanistic pathway toward cyclobutane formation, while the thermal conditions – which still may afford predominantly cyclobutanes – are unable to follow a single pathway to product formation, and may also favor multiple products and/or stereo/regiochemistry. We attributed the combined results to the ability of UV light to affect the polymerization mechanism in the wake of monomeric units already being geometrically confined under extreme conditions.

The "destraightening" seen upon pressure release for thermally produced threads is expected to operate also in photochemically produced threads, likely with a somewhat smaller size due to the better structural order of the photochemical material. Taking this into account (and also noting the absence of thermal expansion in the theoretical thread packing geometries), we apply a 0.5–0.8 Å shift to the experimental *d*-spacings in comparing to theory predictions for defect-free threads at zero pressure (Figure 9). With this correction, the experimental *d*-spacings are consistent with those of the simulated CB-linked *syn-1* and *syn-2* threads. The stereochemistry of the *syn* threads, meaning *cis* hydrogens along the backbone, is consistent with the photochemically mediated [π2s + π2s] cycloaddition outcomes seen in small molecules. Such [π2s + π2s] cycloaddition reaction is favored not only by strain minimization but also by orbital symmetry under photochemical conditions, consistent with production of a more ordered product than for the non-photochemical counterpart. While *anti*-threads consist of photochemically symmetry forbidden [π2s + π2a] cycloaddition, it cannot be ruled out by comparing *d*-spacings between simulation and experiment, *anti*-threads tend to be 0.25 to 0.5 eV per precursor higher in enthalpy than CB-*syn*-threads from 0 to 20 GPa due to the strain of [π2s + π2a] bonds. CB-*syn*-threads are much more likely to be the reaction product under photochemical conditions.

CONCLUSIONS

Herein, we disclose the synthesis of cyclobutane-linked nanothreads, derived from the non-planar and non-aromatic sp^2-rich precursor cyclohexadiene. Whereas each cyclohexadiene isomer is separately compressed at ambient temperature, affording sp^3-enriched polymers, only the 1,4-diene achieved products that are one-dimensional and crystalline, likely owing to fewer viable reaction pathways being plausible. X-ray diffraction obtained on the products of thermal activation demonstrated two visible interplanar spacings ($d_{24\text{-hour}}$ = 5.83 and 6.04 Å and $d_{96\text{-hour}}$ = 4.90 and 6.14 Å). Comparison to simulated diffraction data supports multiple fully saturated products bearing zigzag and armchair arrangements, with the more elliptical cross-section supporting cyclobutane linkages.

The reactivity of 1,4-cyclohexadiene was further investigated using photochemistry. While photochemical activation lowers the required pressure, it also enables a single reaction pathway to emerge: an architecture that propagated through solely [2+2]-cycloadditions is favored, as evidenced by three experimentally observed Friedel pairs (d_{photo} = 4.86, 5.04, and 6.24 Å) that correlate with a highly elliptical cross-section formed from successive cyclobutane formation. The combined provides strong support for the photochemically directed polymerization of 1,4-cyclohexadiene to enable a single reaction pathway to be selected, in close analogy to molecular systems.

Looking forward, the ability to utilize both thermal and photochemical activation modes to direct mechanism and thus, control chemical reactivity under pressure has significant implications for polymer backbone design. Moreover, the integration of both non-aromatic and non-planar monomers into kinetically controlled polymerizations enables a rich variety of hydrocarbon-based materials to be discovered based on commodity chemicals and natural resources. While we demonstrate the ability to dictate reaction mechanism and product formation using photochemistry (in contrast to the observed mixture of products arising from thermal polymerization), we expect many sp^2-rich non-aromatic precursors to demonstrate preferential reaction selectivity under pressure, consistent with traditional organic synthesis.

EXPERIMENTAL METHODS

Materials and Synthesis

A symmetric diamond anvil cell (DAC) with 400 μm culets (type IIA diamonds) were utilized for in situ Raman and infrared spectroscopy experiments. Additionally, a spherical seat DAC with 300 μm culets (Washington diamonds) was utilized for in situ diffraction experiments. Stainless steel gaskets were indented to 45-55 μm thickness. Sample holes of 127 μm in the symmetric DAC and 100 μm in the spherical seat DACs were drilled in the center of the indent using electrical discharge machining and laser drilling.[68] Ruby fluorescence was used as a pressure standard in the in situ experiments.[69]

Prior to use, liquid 1,3-cyclohexadiene (97% from Sigma Aldrich) was filtered through basic alumina to remove the butylated hydroxytoluene (BHT) used as an inhibitor. A drop of the liquid was added to the sample hole and quickly closed and pressurized to 1-2 GPa to avoid evaporation. 1,3-Cyclohexadiene freezes into an amorphous sample under pressure and was compressed in the glassy phase. Liquid 1,4-cyclohexadiene (97% from Sigma Aldrich) was used without further purification. 1,4-Cyclohexadiene solidified by approximately 1.5 GPa and undergoes a molecular phase transition at approximately 4-6 GPa, resulting in a phase distinct from the low-temperature crystal structure. This phase transition results in a polycrystalline sample which was then compressed for the in situ Raman spectroscopy, IR spectroscopy experiments, and nanothread decompression XRD experiments. Cycles of partially melting and recrystallizing the 1,4-cyclohexadiene polycrystals resulted in a powder sample which was compressed for the in situ PXRD experiment.

ASSOCIATED CONTENT

Supporting Information

Synthetic procedures, in situ Raman spectroscopy, IR spectroscopy, X-ray diffraction, polarized light microscopy, X-ray photoelectron spectroscopy, computational methods, packings, and oligomer energies (PDF).

AUTHOR INFORMATION

Corresponding Author

*elizabeth.elacqua@psu.edu

Authors

Morgan Murphy: 0000-0001-9305-8874
Bohan Xu: 0009-0006-6893-0986
Katie E. Rank: 0009-0002-6309-2435
Sikai Wu: 0000-0001-6041-6436
Steven Huss: 0000–0001–6244–4406
John V. Badding: 0000–0002–4517–830X

Steven A. Lopez: 0000-0002-8418-3638
Vincent H. Crespi: 0000–0003–3846–3193
Elizabeth Elacqua: 0000–0002–1239–9560

ACKNOWLEDGMENT

This work was partially funded by the Center for Nanothread Chemistry, a National Science Foundation (NSF) Center for Chemical Innovation (CHE-1832471). Partial support for this project is also through the NSF MRSEC SEED program (DMR-201183). E.E. acknowledges support in the form of an Alfred P. Sloan Foundation grant FG-2021-15490. S. A. L. and K. E. R. thank the NSF for financial support (NSF-OAC-2118201). Portions of this work were performed at HPCAT (Sector 16), Advanced Photon Source (APS), Argonne National Laboratory. HPCAT operations are supported by DOE-NNSA's Office of Experimental Sciences. The Advanced Photon Source is a U.S. Department of Energy (DOE) Office of Science User Facility operated for the DOE Office of Science by Argonne National Laboratory under Contract No. DE-AC02-06CH11357. We thank Guoyin Shen and Changyong Park for their assistance with XRD measurements. This research used 22-IR-1 at the National Synchrotron Light Source II, a U.S. Department of Energy (DOE) Office of Science User Facility operated for the DOE Office of Science by Brookhaven National Laboratory under Contract No. DE-SC0012704. We thank Zhenxian Liu for their assistance with collecting IR data. We thank Jeff Shallenberger of the Materials Characterization Lab in the Materials Research Institute at the Pennsylvania State University for assistance with XPS measurements.

REFERENCES

(1) Schettino, V.; Bini, R. Constraining molecules at the closest approach: chemistry at high pressure. *Chem Soc Rev* **2007**, *36* (6), 869-880.
(2) Ciabini, L.; Santoro, M.; Bini, R.; Schettino, V. High pressure reactivity of solid benzene probed by infrared spectroscopy. *J. Chem. Phys.* **2002**, *116* (7), 2928-2935.
(3) Citroni, M.; Bini, R.; Foggi, P.; Schettino, V. Role of excited electronic states in the high-pressure amorphization of benzene. *Proc. Natl. Acad. Sci. U.S.A.* **2008**, *105* (22), 7658-7663.
(4) Pruzan, P.; Chervin, J. C.; Thiéry, M. M.; Itié, J. P.; Besson, J. M.; Forgerit, J. P.; Revault, M. Transformation of benzene to a polymer after static pressurization to 30 GPa. *J. Chem. Phys.* **1990**, *92* (11), 6910-6915.
(5) Ceppatelli, M.; Santoro, M.; Bini, R.; Schettino, V. High pressure reactivity of solid furan probed by infrared and Raman spectroscopy. *J. Chem. Phys.* **2003**, *118* (3), 1499-1506.
(6) Fitzgibbons, T. C.; Guthrie, M.; Xu, E.-S.; Crespi, V. H.; Davidowski, S. K.; Cody, G. D.; Alem, N.; Badding, J. V. Benzene-derived carbon nanothreads. *Nat. Mater.* **2015**, *14* (1), 43-47.
(7) Li, X.; Baldini, M.; Wang, T.; Chen, B.; Xu, E.-s.; Vermilyea, B.; Crespi, V. H.; Hoffmann, R.; Molaison, J. J.; Tulk, C. A.; et al. Mechanochemical Synthesis of Carbon Nanothread Single Crystals. *J. Am. Chem. Soc.* **2017**, *139* (45), 16343-16349.
(8) Li, X.; Wang, T.; Duan, P.; Baldini, M.; Huang, H.-T.; Chen, B.; Juhl, S. J.; Koeplinger, D.; Crespi, V. H.; Schmidt-Rohr, K.; et al. Carbon Nitride Nanothread Crystals Derived from Pyridine. *J. Am. Chem. Soc.* **2018**, *140* (15), 4969-4972.
(9) Oburn, S. M.; Huss, S.; Cox, J.; Gerthoffer, M. C.; Wu, S.; Biswas, A.; Murphy, M.; Crespi, V. H.; Badding, J. V.; Lopez, S. A.; et al. Photochemically Mediated Polymerization of Molecular Furan and Pyridine: Synthesis of Nanothreads at Reduced Pressures. *J. Am. Chem. Soc.* **2022**, *144* (48), 22026-22034.
(10) Huang, H.-T.; Zhu, L.; Ward, M. D.; Wang, T.; Chen, B.; Chaloux, B. L.; Wang, Q.; Biswas, A.; Gray, J. L.; Kuei, B.; et al. Nanoarchitecture through Strained Molecules: Cubane-Derived Scaffolds and the Smallest Carbon Nanothreads. *J. Am. Chem. Soc.* **2020**, *142* (42), 17944-17955.
(11) Gao, D.; Tang, X.; Xu, J.; Yang, X.; Zhang, P.; Che, G.; Wang, Y.; Chen, Y.; Gao, X.; Dong, X.; et al. Crystalline $C_3N_3H_3$ tube (3,0) nanothreads. *Proc. Natl. Acad. Sci. U.S.A.* **2022**, *119* (17), e2201165119.
(12) Wang, T.; Duan, P.; Xu, E.-S.; Vermilyea, B.; Chen, B.; Li, X.; Badding, J. V.; Schmidt-Rohr, K.; Crespi, V. H. Constraining Carbon Nanothread Structures by Experimental and Calculated Nuclear Magnetic Resonance Spectra. *Nano Lett.* **2018**, *18* (8), 4934-4942.
(13) Duan, P.; Li, X.; Wang, T.; Chen, B.; Juhl, S. J.; Koeplinger, D.; Crespi, V. H.; Badding, J. V.; Schmidt-Rohr, K. The Chemical Structure of Carbon Nanothreads Analyzed by Advanced Solid-State NMR. *J. Am. Chem. Soc.* **2018**, *140* (24), 7658-7666.
(14) Biswas, A.; Ward, M. D.; Wang, T.; Zhu, L.; Huang, H.-T.; Badding, J. V.; Crespi, V. H.; Strobel, T. A. Evidence for Orientational Order in Nanothreads Derived from Thiophene. *J. Phys. Chem. Lett.* **2019**, *10* (22), 7164-7171.
(15) Matsuura, B. S.; Huss, S.; Zheng, Z.; Yuan, S.; Wang, T.; Chen, B.; Badding, J. V.; Trauner, D.; Elacqua, E.; van Duin, A. C. T.; et al. Perfect and Defective ^{13}C-Furan-Derived Nanothreads from Modest-Pressure Synthesis Analyzed by 13C NMR. *J. Am. Chem. Soc.* **2021**, *143* (25), 9529-9542.
(16) Huss, S.; Wu, S.; Chen, B.; Wang, T.; Gerthoffer, M. C.; Ryan, D. J.; Smith, S. E.; Crespi, V. H.; Badding, J. V.; Elacqua, E. Scalable Synthesis of Crystalline One-Dimensional Carbon Nanothreads through Modest-Pressure Polymerization of Furan. **2021**, *15* (3), 4134-4143.
(17) Dunning, S. G.; Chen, B.; Zhu, L.; Cody, G. D.; Chariton, S.; Prakapenka, V. B.; Zhang, D.; Strobel, T. A. Synthesis and Post-Processing of Chemically Homogeneous Nanothreads from 2,5-Furandicarboxylic Acid. *Angew. Chem. Int. Ed.* **2023**, *62* (14), e202217023.
(18) Dunning, S. G.; Zhu, L.; Chen, B.; Chariton, S.; Prakapenka, V. B.; Somayazulu, M.; Strobel, T. A. Solid-State Pathway Control via Reaction-Directing Heteroatoms: Ordered Pyridazine Nanothreads through Selective Cycloaddition. *J. Am. Chem. Soc.* **2022**, *144* (5), 2073-2078.
(19) Tang, W. S.; Strobel, T. A. Evidence for Functionalized Carbon Nanothreads from π-Stacked, para-Disubstituted Benzenes. *J. Phys. Chem. C* **2020**, *124* (45), 25062-25070.
(20) Wang, X.; Yang, X.; Wang, Y.; Tang, X.; Zheng, H.; Zhang, P.; Gao, D.; Che, G.; Wang, Z.; Guan, A.; et al. From Biomass to Functional Crystalline Diamond Nanothread: Pressure-Induced Polymerization of 2,5-Furandicarboxylic Acid. *J. Am. Chem. Soc.* **2022**, *144* (48), 21837-21842.
(21) Ward, M. D.; Tang, W. S.; Zhu, L.; Popov, D.; Cody, G. D.; Strobel, T. A. Controlled Single-Crystalline Polymerization of $C_{10}H_8{\cdot}C_{10}F_8$ under Pressure. *Macromolecules* **2019**, *52* (20), 7557-7563.
(22) Friedrich, A.; Collings, I. E.; Dziubek, K. F.; Fanetti, S.; Radacki, K.; Ruiz-Fuertes, J.; Pellicer-Porres, J.; Hanfland, M.; Sieh, D.; Bini, R.; et al. Pressure-Induced Polymerization of Polycyclic Arene–Perfluoroarene Cocrystals: Single Crystal X-ray Diffraction Studies, Reaction Kinetics, and Design of Columnar Hydrofluorocarbons. *J. Am. Chem. Soc.* **2020**, *142* (44), 18907-18923.
(23) Gerthoffer, M. C.; Wu, S.; Chen, B.; Wang, T.; Huss, S.; Oburn, S. M.; Crespi, V. H.; Badding, J. V.; Elacqua, E. 'Sacrificial' supramolecular assembly and pressure-induced polymerization: toward sequence-defined functionalized nanothreads. *Chem. Sci.* **2020**, *11* (42), 11419-11424.
(24) Gerthoffer, M. C.; Xu, B.; Wu, S.; Cox, J.; Huss, S.; Oburn, S. M.; Lopez, S. A.; Crespi, V. H.; Badding, J. V.; Elacqua, E. Mechanistic insights into the pressure-induced polymerization of

aryl/perfluoroaryl co-crystals. *Polym. Chem.* **2022**, *13* (10), 1359-1368.
(25) Tang, W. S.; Strobel, T. A. Pressure-Induced Solid-State Polymerization of Optically-Tunable Diphenyl-Substituted Diacetylene. *ACS Appl. Polym. Mater.* **2019**, *1* (12), 3286-3294.
(26) Romi, S.; Fanetti, S.; Alabarse, F.; Mio, A. M.; Haines, J.; Bini, R. Towards custom built double core carbon nanothreads using stilbene and pseudo-stilbene type systems. *Nanoscale* **2022**, *14* (12), 4614-4625.
(27) Nobrega, M. M.; Teixeira-Neto, E.; Cairns, A. B.; Temperini, M. L. A.; Bini, R. One-dimensional diamondoid polyaniline-like nanothreads from compressed crystal aniline. *Chem. Sci.* **2018**, *9* (1), 254-260.
(28) Fanetti, S.; Santoro, M.; Alabarse, F.; Enrico, B.; Bini, R. Modulating the H-bond strength by varying the temperature for the high pressure synthesis of nitrogen rich carbon nanothreads. *Nanoscale* **2020**, *12* (8), 5233-5242.
(29) Agati, M.; Romi, S.; Fanetti, S.; Bini, R. High-pressure structure and reactivity of crystalline bibenzyl: Insights and prospects for the synthesis of functional double-core carbon nanothreads. *J. Chem. Phys.* **2023**, *159* (24), 244507.
(30) Hoffmann, R.; Woodward, R. B. Selection Rules for Concerted Cycloaddition Reactions. *J. Am. Chem. Soc.* **1965**, *87* (9), 2046-2048.
(31) Su, H.; Li, X.; Ye, C.; Gao, C.; Sun, X.; Wang, Z.; Dai, R.; Zhang, Z. Confirmation of Phase Transitions and Laser-Assisted Chemical Reaction for Pyridine under High Pressure. *J. Phys. Chem. C* **2022**, *126* (30), 12536-12544.
(32) Chen, D.-F.; Bernsten, S.; Miyake, G. M. Organocatalyzed Photoredox Radical Ring-Opening Polymerization of Functionalized Vinylcyclopropanes. *Macromolecules* **2020**, *53* (19), 8352-8359.
(33) Chen, D.-F.; Boyle, B. M.; McCarthy, B. G.; Lim, C.-H.; Miyake, G. M. Controlling Polymer Composition in Organocatalyzed Photoredox Radical Ring-Opening Polymerization of Vinylcyclopropanes. *J. Am. Chem. Soc.* **2019**, *141* (33), 13268-13277.
(34) Chen, M.; MacLeod, M. J.; Johnson, J. A. Visible-Light-Controlled Living Radical Polymerization from a Trithiocarbonate Iniferter Mediated by an Organic Photoredox Catalyst. *ACS Macro Lett.* **2015**, *4* (5), 566-569.
(35) Kensy, V. K.; Tritt, R. L.; Haque, F. M.; Murphy, L. M.; Knorr Jr, D. B.; Grayson, S. M.; Boydston, A. J. Molecular Weight Control via Cross Metathesis in Photo-Redox Mediated Ring-Opening Metathesis Polymerization. *Angew. Chem. Int. Ed.* **2020**, *59* (23), 9074-9079.
(36) Kottisch, V.; Michaudel, Q.; Fors, B. P. Cationic Polymerization of Vinyl Ethers Controlled by Visible Light. *J. Am. Chem. Soc.* **2016**, *138* (48), 15535-15538.
(37) Ogawa, K. A.; Goetz, A. E.; Boydston, A. J. Metal-Free Ring-Opening Metathesis Polymerization. *J. Am. Chem. Soc.* **2015**, *137* (4), 1400-1403.
(38) Pearson, R. M.; Lim, C.-H.; McCarthy, B. G.; Musgrave, C. B.; Miyake, G. M. Organocatalyzed Atom Transfer Radical Polymerization Using N-Aryl Phenoxazines as Photoredox Catalysts. *J. Am. Chem. Soc.* **2016**, *138* (35), 11399-11407.
(39) Xu, J.; Shanmugam, S.; Fu, C.; Aguey-Zinsou, K.-F.; Boyer, C. Selective Photoactivation: From a Single Unit Monomer Insertion Reaction to Controlled Polymer Architectures. *J. Am. Chem. Soc.* **2016**, *138* (9), 3094-3106.
(40) Chen, B.; Wang, T.; Crespi, V. H.; Li, X.; Badding, J.; Hoffmann, R. All the Ways To Have Substituted Nanothreads. *J. Chem. Theory Comput.* **2018**, *14* (2), 1131-1140.
(41) Valentine, D.; Turro, N. J.; Hammond, G. S. Thermal and Photosensitized Dimerizations of Cyclohexadiene. *J. Am. Chem. Soc.* **1964**, *86* (23), 5202-5208.
(42) Klärner, F.-G.; Dogan, B. M. J.; Ermer, O.; Doering, W. v. E.; Cohen, M. P. Mechanism of the Thermal 1,3-Cyclohexadiene Dimerization: A Non-Concerted Diels-Alder Reaction Leading to the exo-[4+2] Adduct and a Novel [6+4]-Ene Reaction. *Angew. Chem., Int. Ed. Engl.* **1986**, *25* (1), 108-110.
(43) Mella, M.; Fasani, E.; Albini, A. The photosensitized dimerization of 1,3-cyclohexadiene. *Tetrahedron* **1991**, *47* (18), 3137-3154.
(44) Giguere, R. J.; Namen, A. M.; Lopez, B. O.; Arepally, A.; Ramos, D. E.; Majetich, G.; Defauw, J. Studies on tandem ene/intramolecular diels-alder reactions. *Tetrahedron Lett.* **1987**, *28* (52), 6553-6556.
(45) Ahlgren, G.; Åkermark, B. Photodimerisation of 1,4-cyclohexadiene-1,2-dicarboxylic anhydride. *Tetrahedron Lett.* **1974**, *15* (12), 987-988.
(46) Frey, D. A.; Hasegawa, M.; Marvel, C. S. Preparation and aromatization of poly-1,3-cyclohexadiene. II. *J. Polym. Sci., Part A: Gen. Pap.* **1963**, *1* (6), 2057-2065.
(47) Natori, I.; Inoue, S. Anionic Polymerization of 1,3-Cyclohexadiene with Alkyllithium/Amine Systems. Characteristics of n-Butyllithium/N,N,N‘,N‘-Tetramethylethylenediamine System for Living Anionic Polymerization. *Macromolecules* **1998**, *31* (15), 4687-4694.
(48) Hong, K.; Mays, J. W. 1,3-Cyclohexadiene Polymers. 1. Anionic Polymerization. *Macromolecules* **2001**, *34* (4), 782-786.
(49) Lefebvre, G.; Dawans, F. 1,3-Cyclohexadiene polymers. Part I. Preparation and aromatization of poly-1,3-cyclohexadiene. *J. Polym. Sci., Part A: Gen. Pap.* **1964**, *2* (7), 3277-3295.
(50) Marvel, C. S.; Hartzell, G. E. Preparation and Aromatization of Poly-1,3-cyclohexadiene. 1. *J. Am. Chem. Soc.* **1959**, *81* (2), 448-452.
(51) Chen, B.; Hoffmann, R.; Ashcroft, N. W.; Badding, J.; Xu, E.; Crespi, V. Linearly Polymerized Benzene Arrays As Intermediates, Tracing Pathways to Carbon Nanothreads. *J. Am. Chem. Soc.* **2015**, *137* (45), 14373-14386.
(52) Di Lauro, C.; Neto, N.; Califano, S. Vibrational spectrum and normal-mode analysis of 1,3- cyclohexadiene. *J. Mol. Struct.* **1969**, *3* (3), 219-226.
(53) Murray, J. W. The Raman Spectrum of 1,3-Cyclohexadiene. *J. Chem. Phys.* **2004**, *3* (1), 59-60.
(54) We are unable to integrate the C_{sp^3} region as samples oversaturate the detector.
(55) Hagemann, H.; Bill, H.; Joly, D.; Müller, P.; Pautex, N. Raman investigation of 1,4-cyclohexadiene in the liquid and solid state. *Spectrochim. Acta A* **1985**, *41* (5), 751-756.
(56) Perdew, J. P.; Burke, K.; Ernzerhof, M. Generalized Gradient Approximation Made Simple. *Phys. Rev. Lett.* **1996**, *77* (18), 3865-3868.
(57) Grimme, S.; Antony, J.; Ehrlich, S.; Krieg, H. A consistent and accurate ab initio parametrization of density functional dispersion correction (DFT-D) for the 94 elements H-Pu. *J. Chem. Phys.* **2010**, *132* (15), 154104.
(58) Grimme, S.; Ehrlich, S.; Goerigk, L. Effect of the damping function in dispersion corrected density functional theory. *J. Comput. Chem.* **2011**, *32* (7), 1456-1465.
(59) Kresse, G.; Joubert, D. From ultrasoft pseudopotentials to the projector augmented-wave method. *Phys. Rev. B* **1999**, *59* (3), 1758-1775.
(60) Kresse, G.; Hafner, J. Norm-conserving and ultrasoft pseudopotentials for first-row and transition elements. *J. Condens. Matter Phys.* **1994**, *6* (40), 8245.
(61) Kresse, G.; Hafner, J. Ab initio molecular dynamics for liquid metals. *Phys. Rev. B* **1993**, *47* (1), 558-561.
(62) Kresse, G.; Furthmüller, J. Efficiency of ab-initio total energy calculations for metals and semiconductors using a plane-wave basis set. *Comput. Mater. Sci.* **1996**, *6* (1), 15-50.

(63) Kresse, G.; Furthmüller, J. Efficient iterative schemes for ab initio total-energy calculations using a plane-wave basis set. *Phys. Rev. B* **1996**, *54* (16), 11169-11186.
(64) Woodward, R. B.; Hoffmann, R. The Conservation of Orbital Symmetry. *Angew. Chem., Int. Ed. Engl.* **1969**, *8* (11), 781-853.
(65) Jarzynski, C. Nonequilibrium Equality for Free Energy Differences. *Phys. Rev. Lett.* **1997**, *78* (14), 2690-2693.
(66) Woo, T. K.; Margl, P. M.; Blöchl, P. E.; Ziegler, T. A Combined Car−Parrinello QM/MM Implementation for ab Initio Molecular Dynamics Simulations of Extended Systems: Application to Transition Metal Catalysis. *J. Phys. Chem. B* **1997**, *101* (40), 7877-7880.
(67) Oberhofer, H.; Dellago, C.; Geissler, P. L. Biased Sampling of Nonequilibrium Trajectories: Can Fast Switching Simulations Outperform Conventional Free Energy Calculation Methods? *J. Phys. Chem. B* **2005**, *109* (14), 6902-6915.
(68) Hrubiak, R.; Sinogeikin, S.; Rod, E.; Shen, G. The laser micro-machining system for diamond anvil cell experiments and general precision machining applications at the High Pressure Collaborative Access Team. *Rev. Sci. Instrum.* **2015**, *86* (7), 072202.
(69) Shen, G.; Wang, Y.; Dewaele, A.; Wu, C.; Fratanduono, D. E.; Eggert, J.; Klotz, S.; Dziubek, K. F.; Loubeyre, P.; Fat'yanov, O. V.; et al. Toward an international practical pressure scale: A proposal for an IPPS ruby gauge (IPPS-Ruby2020). *High Press. Res.* **2020**, *40* (3), 299-314.

SYNOPSIS TOC (Word Style “SN_Synopsis_TOC”). If you are submitting your paper to a journal that requires a synopsis graphic and/or synopsis paragraph, see the Instructions for Authors on the journal’s homepage for a description of what needs to be provided and for the size requirements of the artwork.

To format double-column figures, schemes, charts, and tables, use the following instructions:

Place the insertion point where you want to change the number of columns
From the **Insert** menu, choose **Break**
Under **Sections**, choose **Continuous**
Make sure the insertion point is in the new section. From the **Format** menu, choose **Columns**
In the **Number of Columns** box, type **1**
Choose the **OK** button

Now your page is set up so that figures, schemes, charts, and tables can span two columns. These must appear at the top of the page. Be sure to add another section break after the table and change it back to two columns with a spacing of 0.33 in.

Table 1. Example of a Double-Column Table

Column 1	Column 2	Column 3	Column 4	Column 5	Column 6	Column 7	Column 8

Authors are required to submit a graphic entry for the Table of Contents (TOC) that, in conjunction with the manuscript title, should give the reader a representative idea of one of the following: A key structure, reaction, equation, concept, or theorem, etc., that is discussed in the manuscript. Consult the journal’s Instructions for Authors for TOC graphic specifications.

Insert Table of Contents artwork here